SISAL FIBERS DEGRADATION IN CEMENT-BASED COMPOSITES: THE EFFECTS OF THERMAL CURING CONDITIONS AND METAKAOLIN CONTENT

INGRID SILVA ASSIS SANTANA, ELLEN CRISTINA BARBOSA MIRANDA, PEDRO JONAS SILVA SANTOS, GESSIVALDO OLIVEIRA CARNEIRO, CLEBER MARCOS RIBEIRO DIAS

Federal University of Bahia – Rua Aristides Novis 02, Federação. 40210-630, Salvador/BA, Brazil.

ABSTRACT

This study employs a 2^3 factorial design to examine the effects of curing time, curing temperature, and metakaolin content on the tensile strength of sisal fibers using the strand-in-cement test. X-ray diffraction (XRD) analysis was also conducted to qualitatively assess the mineralogical composition of the matrices after curing. The results indicated that in matrices without metakaolin, fibers subjected to the highest curing temperature (80°C) and the longest curing time (72 hours) experienced a complete loss of mechanical strength. Even under milder conditions, these fibers showed a reduction in strength compared to the reference fibers. In contrast, matrices with a high metakaolin content (40%) and elevated curing temperatures (80°C) exhibited a significant decrease in the XRD portlandite peak, while the fibers maintained their mechanical integrity. The addition of metakaolin, in combination with higher curing temperatures, appears to be a promising strategy for optimizing sisal fiber-reinforced composite matrices by effectively reducing fiber degradation.

KEYWORDS:

Sisal fibers, 2^k factorial design, cement-based composites, metakaolin, fibers degradation.

1. INTRODUCTION

Brazil is the world's leading producer of sisal fiber, with 90% of the national production concentrated in the state of Bahia (Andrade, Ornelas, & Brandão, 2012). The abundant availability of sisal fibers, combined with their low cost and environmental benefits, distinguishes them from other fiber types (Ferreira et al., 2015). Furthermore, when incorporated into cementitious matrices, plant fibers enhance the mechanical properties of these materials (Castoldi, Souza, & Silva, 2019).

These characteristics make sisal fiber a promising reinforcement option for Portland cement-based composites. However, ensuring the durability of these fibers within such composites remains a significant challenge, as the alkaline conditions of hydrated cement-based matrices can compromise the integrity of plant fibers. Alkaline attack and fiber mineralization are the primary mechanisms leading to composite embrittlement and strength loss in the early stages (Lima, 2004; Wei & Meyer, 2015).

To mitigate fiber degradation caused by the alkaline environment, researchers have explored optimization techniques for matrices and fiber treatments (Castoldi et al., 2022; Amaral, Rodrigues, & Poggiali, 2022). One proposed technique involves modifying the matrix by partially replacing Portland cement with highly reactive pozzolanic materials, such as metakaolin, to reduce calcium hydroxide levels (Rocha & Toledo Filho, 2024). Other approaches include mechanical refining of fibers (Sanchez-Echeverri et al., 2021), silane treatment (Tonoli et al., 2013), and hornification - a method that alters fiber structure through cycles of wetting and drying, reducing their water retention capacity by causing swelling (Amaral, Rodrigues, & Poggiali, 2022).

While the use of pozzolans in cementitious matrices is an effective strategy to reduce fiber degradation from alkaline attack, further research is needed to determine the optimal parameters for complete calcium hydroxide

consumption in the early stages. This study aims to investigate the mechanical properties of sisal fibers incorporated into cementitious matrices, both with and without the addition of metakaolin, under various curing conditions. The objective is to assess the impact of these parameters on fiber durability. To achieve this, eleven series were evaluated using a 2^3 factorial design, varying pozzolan content, curing temperature, and curing time.

2. EXPERIMENTAL

2.1 Materials

The materials used in this study were: a) high-early-strength Portland cement (CP V ARI) supplied by Mizu Cimentos, selected for its lack of pozzolanic additives to isolate the effects of metakaolin during experimentation; b) high-purity metakaolin (MK) HP Ultra provided by Metacaulim do Brasil; c) sisal fibers (SF) sourced from Valente, Bahia, Brazil; and d) deionized water (W). The sisal fibers underwent a hornification process, which involved five wetting-drying cycles. Each wetting cycle lasted 3 hours, followed by drying in an oven at 60°C for 24 hours. After hornification, the fibers exhibited a tensile strength of 317.80 ± 36.16 MPa (see method in 2.2.3), a skeletal density of 1.500 ± 0.045 g/cm³ as determined by helium gas pycnometry, and a crystallinity of 72.5% as measured by X-ray diffraction (XRD).

Table 1 provides the chemical composition and physical properties of CP V ARI cement and MK, determined by X-ray fluorescence (XRF) using a Bruker S2 Ranger spectrometer. The table also includes data on the skeletal densities, specific surface areas, and median equivalent diameters (D_{50}) of the particulate materials, measured using an AccuPyc II 1340 Micromeritics helium gas pycnometer, a Gemini VII Micromeritics analyzer, and a PSA 1190L particle size analyzer, respectively. Additionally, the pozzolanic activity of MK was evaluated using the modified Chapelle test, with the results also presented in Table 1.

Table 1. Chemical composition and physical properties of CPV ARI cement and Metakaolin (MK).

	Determination	CP V ARI	MK
Chemical composition (w/w %)	SiO_2	25.62	44.88
	Al_2O_3	53.23	42.86
	Fe_2O_3	3.50	4.82
	K_2O	3.21	0.72
	SO_3	0.90	0.13
	MgO	3.72	0.67
	MnO	4.1	0.11
	CaO	0.03	---
	Others	0.21	1.58
Loss on ignition at 1000 °C		5.98	4.23
Skeletal density (g/cm³)		3.140 ± 0.014	2.640 ± 0.030
BET surface área (m²/g)		1.46	21.3
D_{50} (µm)		12.49	16.10
Pozzolanic activity (mgCaO/g)		---	879 ± 26

2.2 Methods

2.2.1 Factorial design

A 2^k factorial design was employed to investigate the effects of curing parameters and metakaolin content on the degradation of sisal fibers in cement-based matrices. The design included three numerical factors: curing temperature (T), curing time (t), and the percentage of metakaolin (MK%) as a replacement for Portland cement by weight (see Table 2). A center point (0) was incorporated into the experimental design to evaluate second-order effects and provide an independent estimate of experimental error. Three replicates were conducted at the

center point to detect potential curvature in the responses and assess repeatability, resulting in a total of eleven series. The series were produced in random order to ensure independence of experimental errors.

The durability analysis of sisal fibers was conducted by embedding strands of fibers in cementitious matrices using the "strand-in-cement" test, as proposed by Wei and Meyer (2014). This method involves bundling twenty sisal fibers, securing the ends with adhesive tape, placing the bundle into a cylindrical mold with an internal diameter of 30 mm and a length of 70 mm, and then pouring the matrix around the central portion of the fibers. To facilitate the extraction of the fibers from the hardened block after testing, the fiber bundle is wrapped in wire mesh. Figure 1 shows the setup for the exposure test, including the mold dimensions and the arrangement of the fiber bundles.

Immediately after molding, the specimens were protected and cured in a water bath for the specified duration and at the temperature listed in Table 2. After the curing period, the specimens were demolded, the hardened matrix surrounding the fiber bundles was carefully removed, and the fiber assemblies were extracted for evaluation. The experimental responses measured included the mineral composition of the matrices using XRD and the tensile strength (St) of the sisal fibers. The methods for these measurements are detailed in the following sections.

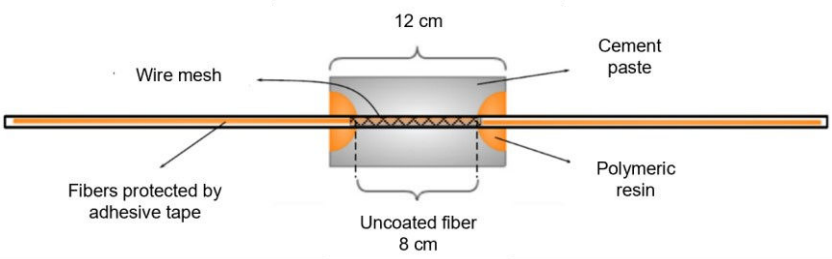

Figure 1. Schematic drawing of specimen for the strand-in-cement test.

Table 2. Experimental series and respective level of factors.

Series		Codified level of factors			Actual level of factors		
Run order	**Name**	**MK**	**T**	**t**	**MK (%)**	**T (°C)**	**t (h)**
S10	MK40%_80°C_72H	+1	+1	+1	40	80	72
S2	MK40%_80°C_24H	+1	+1	-1	40	80	24
S7	MK40%_25°C_72H	+1	-1	+1	40	25	72
S8	MK40%_25°C_24H	+1	-1	-1	40	25	24
S6	MK0%_80°C_72H	-1	+1	+1	0	80	72
S11	MK0%_80°C_24H	-1	+1	-1	0	80	24
S3	MK0%_25°C_72H	-1	-1	+1	0	25	72
S9	MK0%_25°C_24H	-1	-1	-1	0	25	24
S1	MK20%_52.5°C_48H	0	0	0	20	52.5	48
S4	MK20%_52.5°C_48H	0	0	0	20	52.5	48
S5	MK20%_52.5°C_48H	0	0	0	20	52.5	48
Minimum		**-1**	**-1**	**-1**	**0**	**25**	**24**
Maximum		**+1**	**+1**	**+1**	**40**	**80**	**72**

2.2.2 Analysis of the matrices by XRD

The hardened matrices from each series listed in Table 2 were ground into a fine powder and subjected to a solvent exchange process to halt hydration, adapted from Scrivener (2016). Approximately 1g of the powdered paste was mixed with 50 mL of isopropyl alcohol and stirred for 30 minutes. The mixture was then vacuum filtered, dried at 40°C for 10 minutes, and analyzed using X-ray diffraction (XRD) to identify the crystalline phases formed under different curing conditions.

The mineral composition of each matrix was determined using powdered samples with particle sizes of 2-5 µm. These samples were exposed to a monochromatic X-ray beam using a Bruker D2 Phaser diffractometer equipped

with a copper target (wavelength: 0.15406 nm), operating at 30 kV and 10 mA. The crystalline phases present in the samples were identified using HighScore software in conjunction with the COD (Crystallography Open Database).

2.2.3 Tensile tests of sisal fibers

For the mechanical characterization of the vegetable fibers, a direct tensile test was conducted according to ASTM C1557 (2014), which provides the maximum stress, strain at failure, and modulus of elasticity of the fibers. The tests were performed on ten specimens, with outliers discarded based on a normal distribution criterion with a 95% confidence interval ($\mu + 2\sigma$). Figure 7 illustrates the specimen preparation procedure. The tests were carried out using a universal testing machine, model EMIC 23-5D, INSTRON, equipped with a 5 kN load cell and a displacement rate set at 0.2 mm/min.

Tensile strength calculations were performed using the load and displacement data recorded by the testing machine's BlueHill software. The cross-sectional area of the fibers (mm^2), approximated as a circumference, was determined by measuring the diameters with an Olympus TH4-100 optical microscope, taking the average of three readings along the length of each fiber.

3. RESULTS

3.1 Phases assemblage in the matrices

Figure 2 shows the X-ray diffractograms for the matrices from the experimental series after curing in the strand-in-cement test. Table 3 provides a list of all identified crystalline phases.

Brownmillerite, C_2S, and C_3S were identified in all series, implying that even under the most favourable curing conditions - higher temperatures and extended curing times, these phases did not fully hydrate. The absence of C_3A can be attributed to its high reactivity and complete hydration under the curing conditions employed. In the context of vegetable fiber-reinforced composites, the presence of C_2S and C_3S after curing is undesirable, as the subsequent hydration of these phases will produce CH, leading to alkaline attack on the sisal fibers.

Calcite, quartz, periclase, and dolomite were also found in all samples. The intensity of the primary calcite peak ($2\theta = 29.4°$) remained relatively constant across all series, as shown in Figure 2c. Conversely, the intensity of the primary quartz peak ($2\theta = 26.64°$), a phase present in metakaolin (see 2.1), increased proportionally with the amount of metakaolin replacing cement.

Among the hydration products, portlandite, ettringite, and monosulfate were commonly detected. Figure 2a shows that the characteristic ettringite peaks (2θ = 9.09°, 15.78°, and 22.94°) are present in the diffraction patterns of series S3, S7, S8, and S9, which were cured at 25°C. In contrast, series S11 and S6, cured at 80°C, exhibit broad, diffuse peaks between 2θ = 8.5° and 10.5°, suggesting the formation of meta-ettringite ($3CaO.3CaSO_4.Al_2O_3.12H_2O$) (Zhou; Lachowski; Glasser, 2004).

The literature presents conflicting findings regarding the temperature at which ettringite decomposes. Lothenbach et al. (2007) found that ettringite decomposes completely at 50°C after 20 hours, suggesting that it is unstable above this temperature in cement pastes. Carmona-Quiroga; Blanco-Varela, (2013) reported that ettringite decomposes at temperatures exceeding 65°C after 20 hours under isothermal conditions. Collepardi (2003) found that ettringite dehydrates completely above 70°C under steam curing, making it unstable (Elkhadiri; Puertas, 2008). Building on this, Taylor, Famy, and Scrivener (2001) reported the formation of delayed ettringite (DEF) in hydrated cement mixtures, particularly in systems with high permeability, sulfate-rich environments, and the presence of water (Katsioti et al., 2011).

Hemicarboaluminate formation was observed in series S7, S8, S9, and S3, cured at 25°C, resulting from the interaction of alumina from C_3A with limestone and portlandite (Zunino; Scrivener, 2021). The addition of metakaolin, an aluminate source, further promoted hemicarboaluminate formation by reacting with calcium carbonate and portlandite (Zunino; Scrivener, 2021). This is supported by the analysis of series S7 and S8, showing an increased intensity of the hemicarboaluminate peak in Figure 2a and a decreased intensity of the portlandite peak in Figures 2 and 2c.

In series S1, S2, S4, S5, and S10 (Figure 2a), the absence of ettringite and hemicarboaluminate is attributed to curing at temperatures exceeding 50°C. Additionally, a poorly resolved peak at 2θ = 9.22° is observed in these series, which could be associated with the presence of chabazite ($CaAl_2.Si_4O_{12}.6H_2O$), a zeolite, or possibly related to the unexpected formation of thaumasite ($3CaO.SiO_2.CO_3.SO_4.12H_2O$).

Thaumasite formation can occur through the incorporation of Si^{4+} into the ettringite structure, replacing Al^{3+} ions in the $Ca_6[Al(OH)_6]_2$ columns and substituting $[(SO_4)_3.2H_2O]$ with $[(SO_4)_2.(CO_3)_2]$ (Irassar et al., 2005; Pipilikaki et al., 2008). Alternatively, it may form through interactions between sulfates and carbonates in the pore solution and the C-S-H gel (Pipilikaki et al., 2008).

Pipilikaki et al. (2008) suggested that high humidity can facilitate the transport of ions required for the formation of thaumasite, and thus, the thermal curing in this study may have enhanced ion transport. Furthermore, several studies have shown that low temperatures (0-25°C) favor thaumasite formation due to the increased solubility of calcium salts involved in its synthesis (Ma et al., 2006; Matschei; Glasser, 2015; Pipilikaki et al., 2008; Wimpenny; Slater, 2003). Figure 2a indicates that series S1, S2, S4, S5, and S10 may be releasing calcium, sulfate, and carbonate ions from the decomposition of ettringite and hemicarboaluminate at temperatures above 50°C.

The thermal stability of thaumasite is reported inconsistently in the literature. Matschei and Glasser (2015) note decomposition beginning at 69°C, while Macphee and Diamond (2003) suggest stability only up to 30°C. In contrast, Bellmann and Bensted (2003, 2006) claim that thaumasite remains stable up to 110°C. Schmidt et al. (2008) propose that thaumasite's thermodynamic stability is highly dependent on the pH of the medium. Stronger interactions between cement and sulfate solutions can lower the pH of the pore water, promoting thaumasite stability at higher temperatures. This pH reduction may result from the consumption of calcium hydroxide (CH) during pozzolanic reactions.

Lothenbach et al. (2017) demonstrated that the high pH and alkalinity of cement mix water can dissolve aluminosilicates, leading to the formation of zeolites such as chabazite. This phenomenon was observed in mixtures containing 20% or more metakaolin, where the decomposition of ettringite began at 52.5°C. The release of calcium, sulfate, and silicon promoted the formation of chabazite, particularly in series S2 and S10. When the sulfate-to-calcium ratio exceeds 1, calcium-containing solids like C-S-H and chabazite are likely to form. Additionally, an increase in silicon content further enhances the formation of chabazite (Figure 2a).

Figure 2b shows that series S3, S6, and S11, which lack metakaolin and were cured at 80°C, exhibited more intense diffraction peaks for calcium hydroxide [$Ca(OH)_2$] at 2θ angles of 17.99°, 34.02°, and 46.98°. According to Escalante-García and Sharp (2001), increasing the temperature can accelerate the hydration of anhydrous phases. However, as the metakaolin content and curing temperature increased, a gradual reduction in the amount of portlandite was observed. This reduction can be attributed to pozzolanic reactions, where the hydrolysis of pozzolanic materials and the breakdown of the silicate and aluminosilicate network release calcium, silicon, and aluminum ions. These ions then react with water and calcium hydroxide to form C-S-H (calcium-silicate-hydrate gel) and calcium and aluminum hydroxides (such as C_2ASH_8, C_4AH_{13}, and C_3AH_6), as described by Lothenbach, Scrivener, and Hooton (2011). The formation of these new hydrated phases, at the expense of portlandite, indicates that the pozzolanic reactions consumed the calcium hydroxide released during cement hydration.

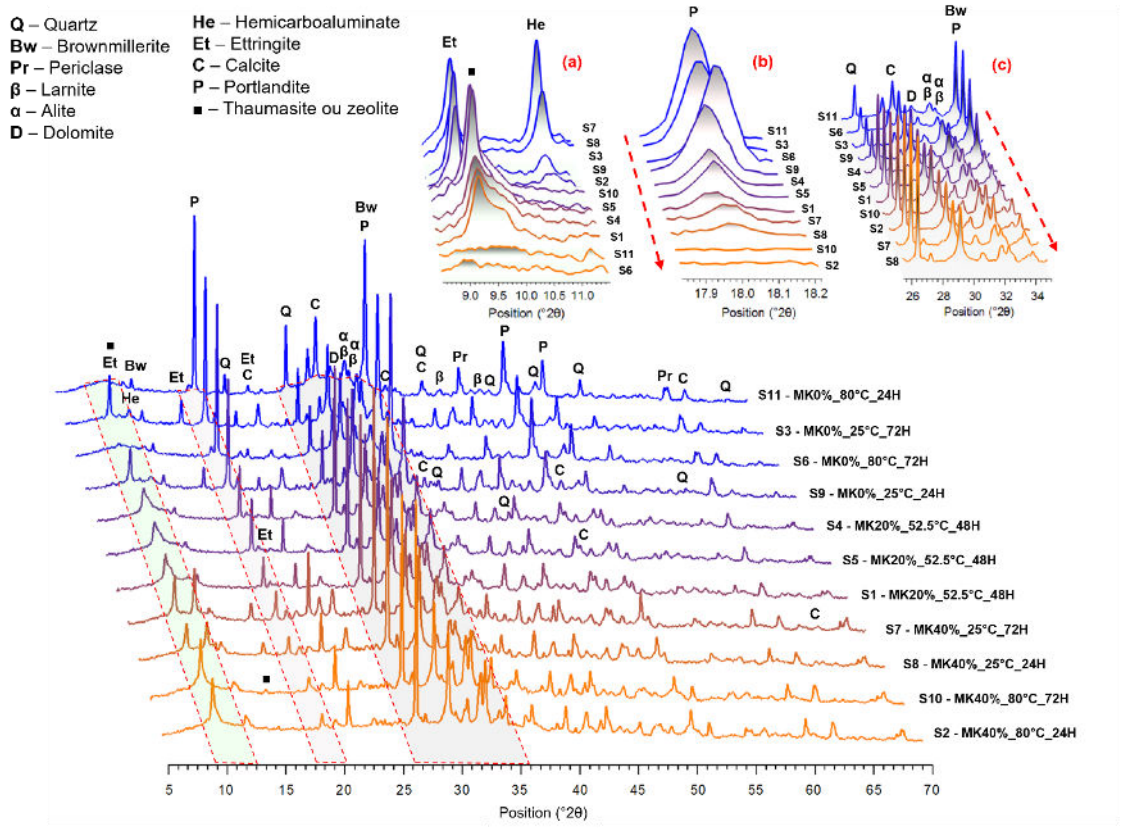

Figure 2 – XRD patterns of the matrices.

Table 3 – Results of qualitative phase analysis of matrices and corresponding tensile strength of fibers.

Series		Phases by qualitative XRD analysis[a]											S_t (MPa)
		β	*α*	*Bw*	*Pr*	*C*	*Q*	*Et*	*Z*	*Th*	*P*	*He*	
MK40%_80°C_72H	S10	■	■	■	■	■	■	▭	■	■			296 ± 29
MK40%_80°C_24H	S2	■	■	■	■	■	■	▭	■	■			297 ± 20
MK40%_25°C_72H	S7	▭	▭	■	■	■	■	■			▭	■	141 ± 59
MK40%_25°C_24H	S8	▭	▭	■	■	■	■	■			▭	■	239 ± 16
MK0%_80°C_72H	S6	▭	▭	■	■	■	■		▭	▭	■		---
MK0%_80°C_24H	S11	▭	▭	■	■		■		▭	▭	■		---
MK0%_25°C_72H	S3	■	■	■	■	■	■	■			■	▭	99 ± 13
MK0%_25°C_24H	S9	■	■	■	■	■	■	■			■	▭	97 ± 43
MK20%_52.5°C_48H	S1	▭	▭	■	■	■	▭		■	■	▭		227 ± 31
MK20%_52.5°C_48H	S4	▭	▭	■	■	■	▭		■	■	■		113 ± 65
MK20%_52.5°C_48H	S5	▭	▭	■	■	■	▭		■	■	■		157 ± 22
Minimum		---											**0**
Maximum		---											**297**

[a] *β– Larnite, α - Alite; Bw - brownmillerite; Pr - Periclase; C - Calcite, Q - Quartz, Et - ettringite, Z - Zeolite, Th - Thaumasite, P - Portlandite, He - Hemicarboaluminate.*

▭ Low intensity ■ Moderate intensity ■ Strong intensity ▭ Traces ▭ Absence

3.2 Tensile strength

Figure 3 presents the tensile stress-strain curves for the fibers evaluated in each series of the factorial design. The results display four fibers per series, with the corresponding average curve highlighted. Curves that showed excessive deformation at constant stress levels, suggesting fiber slippage, were excluded from the analysis. After filtering the appropriate curves, the average tensile strengths of the fibers were calculated.

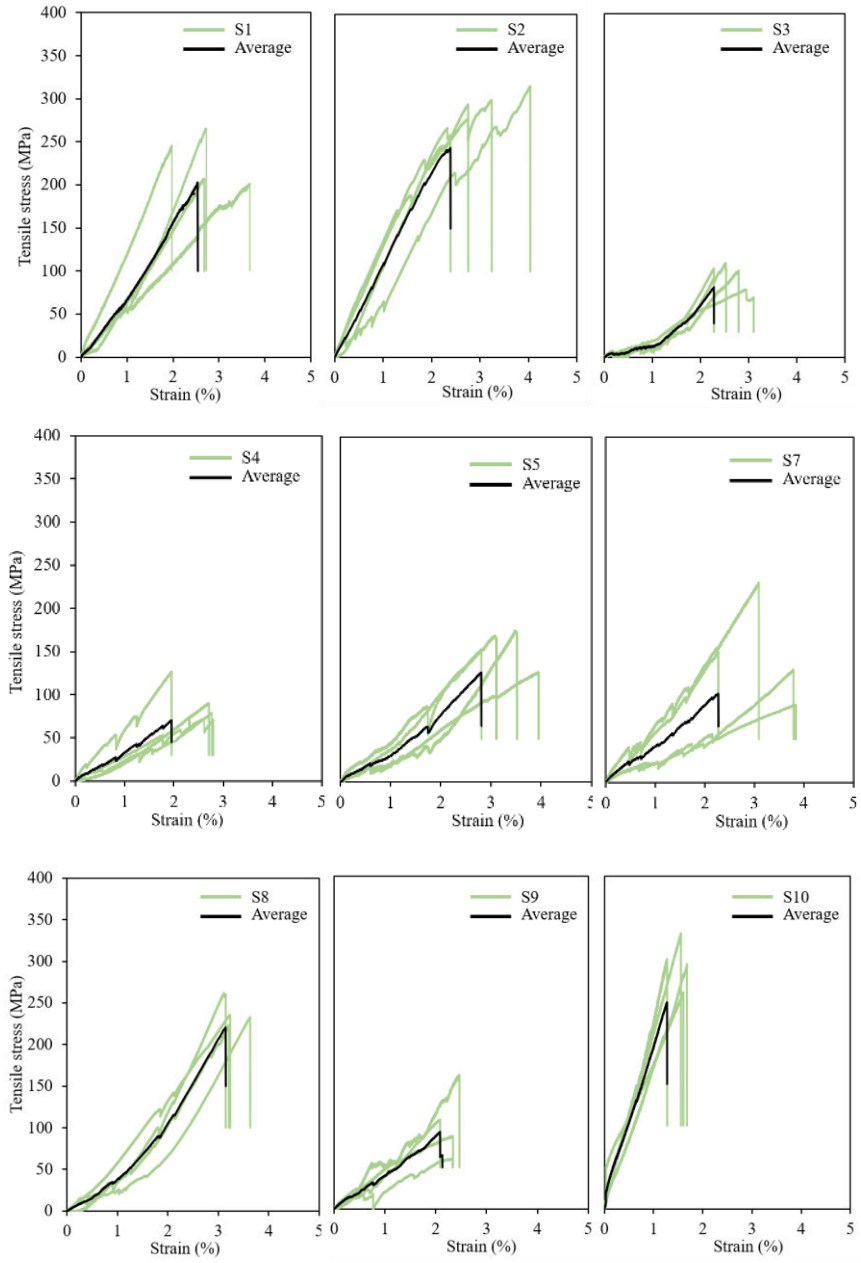

Figure 3. Tensile stress-strain curves for fibers following the strand-in-cement test (See Table 2).

Fibers exposed to cement matrices without pozzolan exhibited lower mechanical strength compared to those embedded in matrices with metakaolin, confirming the negative impact of high alkalinity environments on the durability of vegetable fibers and the beneficial effect of the pozzolanic reaction in mitigating fiber degradation in such environments. Fibers from series MK0%_80°C_72H (S6) and MK0%_80°C_24H (S11), cured at 80°C were completely degraded, making it impossible to evaluate their mechanical strength.

The relationship between the direct tensile strength of the fibers, metakaolin content, and curing temperature of the mixture is represented by Equation 1. This Equation is statistically significant (α = 0.05) with a non-significant lack of fit and presents an R^2 equal to 0.8873 and R^2_{adj} equal to 0.8390. ANOVA showed that curing time parameter did not have a significant effect on tensile strength of fibers.

$$\sigma = 147.875 - 1.782 \times T - 0.0239 \times M + 0.093 \times T \times M \quad (1)$$

Where, σ is the tensile strength of fibers, in MPa, T is the cure temperature, in °C, and M is the metakaolin content, in %.

Figure 4 illustrates the response surface for the tensile strength of fibers, highlighting the synergistic effect between temperature and metakaolin content. For formulations without pozzolan cured at 25°C, fibers lost strength compared to hornified fibers (317.80 ± 36.16 MPa) prior to the strand-in-cement test. The figure also shows that in formulations without pozzolan, fiber strength decreases as the temperature rises, leading to complete disintegration of fibers at 80°C (see S6 and S11 series in Table 3). In contrast, for formulations with 40% pozzolan, higher temperatures enhance mechanical performance due to their influence on matrix hydration reactions.

The effect of temperature alone on fiber strength was not statistically significant. However, using pozzolan as a partial replacement for cement improves fiber tensile strength, likely due to the consumption of calcium hydroxide. Higher curing temperatures accelerate pozzolanic reactions, reducing calcium hydroxide in the matrix (Deschner, Lothenbach, & Neubauer, 2013; Santana, Ribeiro, & Dias, 2022). Thus, combining metakaolin with high curing temperatures can optimize the matrix and enhance the durability of sisal fiber-reinforced cement composites

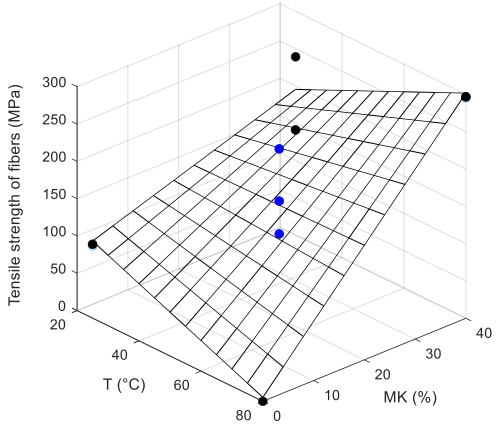

Figure 4. Response surface for tensile strength of fibers (center point results in blue).

4. CONCLUSIONS

Based on the mineralogical analysis of cement matrices and tensile tests conducted on fibers exposed to cement matrices, with and without metakaolin additions, under varying curing conditions, the following conclusions were drawn:

a) The tensile strength of the fibers is significantly influenced by the pozzolan content, showing a directly proportional relationship. At higher pozzolan levels, elevated curing temperatures help maintain fiber strength, whereas at lower pozzolan levels, increased temperatures can lead to fiber degradation.

b) The reduction in calcium hydroxide (CH) content in matrices with high metakaolin content and elevated curing temperatures aligns with the mechanical test results, indicating an accelerated pozzolanic reaction under these conditions. The combination of maximum metakaolin content and high curing temperatures promotes an accelerated pozzolanic reaction and early consumption of CH.

c) Utilizing metakaolin combined with higher curing temperatures is an effective strategy to accelerate the strength gain of composites while mitigating fiber degradation. However, the presence of remaining anhydrous cement phases should be considered, as they may lead to the formation of calcium hydroxide over time, contributing to potential fiber degradation.

ACKNOWLEDGEMENTS

The authors acknowledge the financial support of CNPq (Process n° 309270/2022-7; Process n° 404262/2023-6 and the Laboratório de Ensaios em Durabilidade dos Materiais (LEDMa) of the Federal University of Bahia.

REFERENCES

Andrade, R., Ornelas, J. and Brandão, W. 2012. Situação atual do sisal na Bahia e suas novas possibilidades de utilização e aproveitamento. Comunicação SEAGRI, p. 14-19.

Amaral, L. M., Rodrigues, C. S. and Poggiali, F. S. J. 2022. Hornification on vegetable fibers to improve fiber-cement composites: A critical review. Journal of Building Engineering, *48*, 103947.

American Society for Testing and Materials. 2014. ASTM C1557: Standard Test Method for Tensile Strength and Young's Modulus of Fibers. ASTM international.

Bellmann, F. and Bensted, J. 2006. On the formation of thaumasite $CaSiO_3$ $CaSO_4$ $CaCO_3$ $15H_2O$: Part II. Advances in Cement Research, 18(3), 129–134.

Bensted, J. 2003. Thaumasite—direct, woodfordite and other possible formation routes. Cement and Concrete Composites, 25(8), 873–877.

Carmona-Quiroga, P. M. and Blanco-Varela, M. T. 2013. Ettringite decomposition in the presence of barium carbonate. Cement and Concrete Research, 52, 140-148.

Castoldi, R. S., Souza, L. M. S. and Silva, F. A. 2019. Comparative study on the mechanical behavior and durability of polypropylene and sisal fiber reinforced concretes. Construction and Building Materials, 211, 617-628.

Castoldi, R. S., Souza, L. M. S., Souto, F., Liebscher, M., Mechtcherine, V. and Silva, F. A. 2022. Effect of alkali treatment on physical–chemical properties of sisal fibers and adhesion towards cement-based matrices. Construction and Building Materials, *345*, 128363.

Collepardi, M. 2003. A state-of-the-art review on delayed ettringite attack on concrete. Cement and Concrete Composites, v. 25, n. 4, Concrete Durability, p. 401–407.

Deschner, F., Lothenbach, B., Winnefeld, F. and Neubauer, J. 2013. Effect of temperature on the hydration of Portland cement blended with siliceous fly ash. Cement and concrete research, *52*, 169-181.

Elkhadiri, I. and Puertas, F. 2008. The effect of curing temperature on sulphate-resistant cement hydration and strength. Construction and Building Materials, v. 22, n. 7, p. 1331–1341.

Ferreira, S. R., de Andrade Silva, F., Lima, P. R. L. and Toledo Filho, R. D. 2015. Effect of fiber treatments on the sisal fiber properties and fiber–matrix bond in cement based systems. Construction and Building Materials, 101, 730-740.

Escalante-García, J. I. and Sharp, J. H. 2001. The microstructure and mechanical properties of blended cements hydrated at various temperatures. Cement and Concrete Research, 31(5), 695–702.

Irassar, E. F., Bonavetti, V. L., Trezza, M. A. and González, M. A. 2005. Thaumasite formation in limestone filler cements exposed to sodium sulphate solution at 20 C. Cement and Concrete Composites, 27(1), 77-84.

Katsioti, M., Patsikas, N., Pipilikaki, P., Katsiotis, N., Mikedi, K. and Chaniotakis, M. 2011. Delayed ettringite formation (DEF) in mortars of white cement. Construction and Building Materials, 25(2), 900-905.

Lima, P. R. L. 2004. Análise teórica e experimental de compósitos reforçados com fibras de sisal. Tese (Doutorado em Engenharia Civil) – Universidade Federal do Rio de Janeiro, Rio de Janeiro.

Lothenbach, B., Winnefeld, F., Alder, C., Wieland, E. and Lunk, P. 2007. Effect of temperature on the pore solution, microstructure and hydration products of Portland cement pastes. Cement and Concrete Research, *37*(4), 483-491.

Lothenbach, B., Bernard, E. and Mäder, U. 2017. Zeolite formation in the presence of cement hydrates and albite. Physics and Chemistry of the Earth, Parts A/B/C, 99, 77-94.

Lothenbach, B., Scrivener, K. and Hooton, R. D. 2011. Supplementary cementitious materials. Cement and Concrete Research, 41(12), 1244–1256.

Ma, B., Gao, X., Byars, E. A. and Zhou, Q. (2006). Thaumasite formation in a tunnel of Bapanxia Dam in Western China. Cement and Concrete Research, *36*(4), 716-722.

Macphee, D. and Diamond, S. 2011. Thaumasite in Cementitious Materials. Cement and Concrete Composites, 25(8), 805–807.

Matschei, T. and Glasser, F. P. 2015. Thermal stability of thaumasite. Materials and Structures, 48(7), 2277–2289.

NP P18-513. 2010. Metakaolin. Pozzolanic addition for concrete. Definitions, specifications and conformity criteria. Association Française de Normalisation, La Plaine Saint-Denis, (in French).

Rocha, J. H. A. and Toledo Filho, R. D. 2024. Microstructure, hydration process, and compressive strength assessment of ternary mixtures containing Portland cement, recycled concrete powder, and metakaolin. Journal of Cleaner Production, *434*, 140085.

Pipilikaki, P., Papageorgiou, D., Teas, C., Chaniotakis, E. and Katsioti, M. 2008. The effect of temperature on thaumasite formation. Cement and Concrete Composites, *30*(10), 964-969.

Pourchez, J., Valdivieso, F., Grosseau, P., Guyonnet, R. and Guilhot, B. 2006. Kinetic modelling of the thermal decomposition of ettringite into metaettringite. Cement and concrete research, *36*(11), 2054-2060.

Sanchez-Echeverri, L. A., Ganjian, E., Medina-Perilla, J. A., Quintana, G. C., Sanchez-Toro, J. H. and Tyrer, M. 2021. Mechanical refining combined with chemical treatment for the processing of Bamboo fibres to produce efficient cement composites. Construction and Building Materials, 269, 121232.

Santana, I. S. A., Ribeiro, D. V. and Dias, C. M.R. 2022. Otimização da cura visando a aceleração do consumo de hidróxido de cálcio em matrizes cimentícias contendo pozolanas. 4º Congresso Luso-Brasileiro de Materiais de Construção Sustentáveis (CLBMCS).

Scrivener, K., Snellings, R., Lothenbach, B. and Press, C. R. C. 2016. A practical guide to microstructural analysis of cementitious materials. Vol. 540. Boca Raton, FL, USA: Crc Press.

Schmidt, T., Lothenbach, B., Romer, M., Scrivener, K., Rentsch, D. and Figi, R. 2008. A thermodynamic and experimental study of the conditions of thaumasite formation. Cement and Concrete Research, 38(3), 337-349.

Taylor, H. F. W, Famy, C. and Scrivener, K. L. 2001. Delayed ettringite formation. Cement and Concrete Research, v. 31, n. 5, p. 683–693.

Tonoli, G. H. D., Belgacem, M. N., Siqueira, G., Bras, J., Savastano Jr, H. and Lahr, F. R. 2013. Processing and dimensional changes of cement based composites reinforced with surface-treated cellulose fibres. Cement and Concrete Composites, 37, 68-75.

Wei, J. and Meyer, C. 2015. Degradation mechanisms of natural fiber in the matrix of cement composites. Cement and concrete Research, v. 73, p. 1-16.

Wimpenny, D. and Slater, D. 2003. Evidence from the highways agency thaumasite investigation in Gloucestershire to support or contradict postulated mechanisms of thaumasite formation (TF) and thaumasite sulfate attack (TSA). Cement and Concrete Composites, 25(8), 879–888.

Zhou, Q., Lachowski, E. E. and Glasser, F. P. 2004. Metaettringite, a decomposition product of ettringite. Cement and Concrete Research, 34(4), 703-710.

Zunino, F. and Scrivener, K. 2021. The reaction between metakaolin and limestone and its effect in porosity refinement and mechanical properties. Cement and Concrete Research, v. 140, p. 106307.